SSRG International Journal of Mechanical Engineering
ISSN: 2348-8360/ https://doi.org/10.14445/23488360/IJME-V12I8P103

Volume 12 Issue 8, 20-27, August 2025

Original Article

Optimization Analysis of Ship Windlass Drum Based on RSM

Xiaoyu Liu[1], Aldrin Calderon[2], Ruichen Tian[3]

[1,2,3]*School of Mechanical, Manufacturing, and Energy Engineering, Mapúa University, Manila, Philippines.*
[1]*School of Intelligent Manufacturing Engineering, Qingdao Huanghai University, Qingdao, China.*

[2]*Corresponding Author : adcalderon@mapua.edu.ph*

Received: 05 June 2025 Revised: 05 July 2025 Accepted: 06 August 2025 Published: 29 August 2025

Abstract *- This paper focuses on the optimization analysis of the winch drum in a ship anchoring machine using the Response Surface Method (RSM). A detailed analysis of its working principle and force conditions is conducted. Based on this, a high-accuracy finite element model is established in ANSYS Workbench. RSM is then applied to construct objective and surrogate models, enabling the exploration of the relationship between design variables and performance metrics. Through optimization, the stress distribution is significantly improved, the maximum equivalent stress is reduced, and material utilization is enhanced. These improvements contribute to the structural reliability and efficiency of the anchoring system, offering valuable guidance for engineering applications.*

Keywords *- Winch drum of marine anchoring machines, Optimization analysis, Modelling analysis, Response surface methodology.*

1. Introduction

In the present era of globalisation, marine transport is a crucial enabler of global trade, accounting for approximately 80% of the world's cargo transportation. Ships, as the primary carriers of marine logistics, must meet stringent requirements for safety and reliability.

Fig. 1 Ratchet-type anti-impact reel

Among the critical systems ensuring ship safety, the anchor winch plays an irreplaceable role in enabling secure mooring and controlled anchoring operations. As the core transmission element, the winch drum is subjected to complex loading conditions during operations, and any structural weakness could lead to serious safety incidents [1].

Traditional drum designs often fail to reconcile load-bearing capacity, structural safety, and lightweight efficiency-particularly under repetitive anchoring cycles and harsh marine conditions [2]. A key challenge is uncontrolled rotation during anchor deployment, driven by cable self-weight and traction acceleration [2]. To address this, advanced control strategies such as brake cylinder modulation with linear encoders and gear-change switch modules have been proposed, enabling controllable free release of the drum to reduce shock impact [3].

Additional improvements include the incorporation of ratchet-type brake mechanisms on the opposite side of belt brakes to serve as backstop protection in case of failure [3]. These operational-level innovations, while valuable, do not address the inherent dynamic behaviour and modal characteristics of the drum structure-factors that significantly affect fatigue, resonance risk, and service life.

In recent years, the demand for high-performance and energy-efficient ship components has prompted extensive research into structural optimization techniques. The study emphasized the effectiveness of RSM in solving complex nonlinear problems while reducing computational cost [4]. Drawing on these insights, this study focuses on the optimization analysis of a ship windlass drum structure using RSM to achieve weight reduction and improved mechanical performance under operational constraints.

Computational advancements have enabled Finite Element Analysis (FEA) and theoretical mechanics to evaluate winch stress and deformation [5]. This has laid the foundation for optimization strategies targeting weight reduction and structural reliability, such as response surface methods and evolutionary algorithms. Nevertheless, existing studies tend to focus on static strength or control systems, with insufficient attention to modal response and dynamic characteristics under anchoring load profiles [6].

1.1. Research Gap and Novelty

Despite existing contributions, there remains a clear research gap in combining modal analysis with structural optimization for marine anchor winch drums. Modal behaviour-including natural frequencies, mode shapes, and deformation patterns-can significantly influence structural safety and vibration resistance but has not been fully explored in prior work [7, 8].

This study aims to fill this gap by:

- Performing a comprehensive modal analysis on a typical anchor winch drum.
- Identifying critical modes affecting stability and fatigue.
- Integrating lightweight optimization based on modal responses.
- Applying MOGA-based strategies to balance stiffness, weight, and vibration performance.

Compared with studies focusing solely on response surfaces, structural improvement, or modular design, this research offers a novel framework combining dynamic characteristics and multi-objective optimization, contributing to next-generation winch design.

2. Literature Review

Recent studies highlight diverse approaches to winch optimization:

Static and Lightweight Design: Li et al. [1] optimized drum structures via response surfaces, emphasizing stress reduction and weight control. An researcher applied FEA to anchor winches but restricted analysis to static conditions. An advanced lightweight techniques for anchor structures, though dynamic effects were unaddressed.

Zhu et al. [4] conducted an in-depth review on the application of intelligent optimization methods-such as Response Surface Methodology (RSM), surrogate models, and multi-objective algorithms-in ship hull form design.

Modular and Control Systems: Tang et al. [6] proposed modular anchor machinery designs and developed grooved drums to mitigate spooling issues.

Dynamic Behaviour: Analysed vibration patterns in fence-type reels, while Hohmann et al. [7] evaluated contact mechanics in drum brakes using FEA, offering insights into resonance risks.

Zemliak and Espinosa-Garcia [10] compared optimization strategies, informing algorithmic selection. Multi-Objective Optimization: Garcia and González [11] employed evolution strategies for shape optimization, foundational to MOGA applications here.

Notably, Abbes et al. [12] modelled gearbox noise via acoustic-structural coupling, hinting at resonance mitigation strategies for rotating components. Meanwhile, provided mechanical benchmarks through strength analysis of anchor supports.

In summary, while previous studies contribute to understanding winch mechanics, control systems, and lightweighting, few have combined modal safety, pre-stress conditions, gear optimization, and structural integrity into a unified optimization strategy. This study addresses this gap through a novel, integrated approach.

3. First-Order Head in the Structure and Mechanical Model of Anchor Reel

3.1. Load and Boundary Condition

The windlass is subjected to complex and variable loads in the working process, including static loads, dynamic loads and various kinds of special loads, and a full understanding of these loads is the foundation for the derivation of reasonable boundary conditions [12].

According to the general theorem of continuum mechanics, the equilibrium equations of this unit are as follows.

$$\begin{Bmatrix} \frac{\partial \sigma_x}{\partial x}+\frac{\partial \tau_y}{\partial y}+\frac{\partial \tau_z}{\partial z}+F_x=0 \\ \frac{\partial \tau_{xy}}{\partial x}+\frac{\partial \sigma_y}{\partial y}+\frac{\partial \tau_{xy}}{\partial z}+F_x=0 \\ \frac{\partial \tau_{xz}}{\partial x}+\frac{\partial \tau_z}{\partial y}+\frac{\partial \sigma_z}{\partial z}+F_x=0 \end{Bmatrix} \quad (1)$$

Or written as

$$\mathrm{A}\sigma + F = 0 \quad (2)$$

In this equation, F represents the body force per unit volume along each principal stress direction, and A represents the differential operator, i.e.,

$$\mathrm{A} = \begin{pmatrix} \frac{\partial}{\partial x} & 0 & \frac{\partial}{\partial y} & 0 \\ 0 & \frac{\partial}{\partial y} & \frac{\partial}{\partial x} & 0 \\ 0 & 0 & \frac{\partial}{\partial z} & \frac{\partial}{\partial y} \\ 0 & 0 & 0 & \frac{\partial}{\partial x} \end{pmatrix} \quad (3)$$

Neglecting the higher-order infinitesimals in the displacement derivatives according to the relevant elements of the small deformation assumption yields the geometric relationship between strain and displacement presented as such.

$$\varepsilon_x = \frac{\partial u}{\partial x}$$

$$\varepsilon_y = \frac{\partial v}{\partial y} \quad (4)$$

$$\varepsilon_z = \frac{\partial w}{\partial y}$$

Or written as

$$\varepsilon = Lu \quad (5)$$

Where L denotes the differential operator, i.e.

$$\mathrm{L} = \begin{pmatrix} \frac{\partial}{\partial x} & 0 & 0 \\ 0 & \frac{\partial}{\partial y} & 0 \\ 0 & 0 & \frac{\partial}{\partial z} \\ \frac{\partial}{\partial y} & \frac{\partial}{\partial x} & 0 \\ 0 & \frac{\partial}{\partial z} & \frac{\partial}{\partial y} \\ \frac{\partial}{\partial z} & 0 & \frac{\partial}{\partial x} \end{pmatrix} = \mathrm{A}^{\tau} \quad (6)$$

According to the generalised elasticity theorem, the expression of the intrinsic model of the compression-tension bilinear modulus in the right-angled coordinate system is presented as:

$$\begin{Bmatrix} \varepsilon_1 \\ \varepsilon_2 \\ \varepsilon_3 \end{Bmatrix} = \begin{Bmatrix} a_{11} & a_{12} & a_{13} \\ a_{21} & a_{22} & a_{23} \\ a_{31} & a_{32} & a_{33} \end{Bmatrix} \begin{Bmatrix} \sigma_1 \\ \sigma_2 \\ \sigma_3 \end{Bmatrix} \quad (7)$$

Or expressed as:

$$\varepsilon_i = \boldsymbol{a}_j \sigma_j (i, j = 1,2,3) \quad (8)$$

In this equation, εi represents the principal strain and σj represents the principal stress, where is the material flexibility matrix, which is also called the flexibility coefficient. If the physical equations are written in the form of principal stresses, then they are:

$$\begin{Bmatrix} \sigma_1 \\ \sigma_2 \\ \sigma_3 \end{Bmatrix} = \begin{Bmatrix} C_{11} & C_{12} & C_{13} \\ C_{21} & C_{22} & C_{23} \\ C_{31} & C_{32} & C_{33} \end{Bmatrix} \begin{Bmatrix} \sigma_1 \\ \sigma_2 \\ \sigma_3 \end{Bmatrix} \quad (9)$$

Or expressed as:

$$\sigma_i = C_\eta \varepsilon_j (i, j = 1,2,3) \quad (10)$$

In this equation, C_{ij} represents the material elasticity matrix, which is inversely related to the material flexibility matrix a_{ij}.

In the hydrostatic analysis of the reel, the main consideration is the tensile force exerted by the anchor chain on the reel, which is related to the type and length of the anchor chain and the condition of the ship in the water, e.g., in the case of the maximum working load, the tensile force on the reel can reach several hundreds of kilo newtons, but this situation means that the effect of dynamic loads due to external forces, such as wind and waves, must not be neglected, and the study has shown that the dynamic loads increase the stress level of the reel. It is concluded that the dynamic load will increase the stress level of the reel to a certain extent, which puts forward higher requirements on the structural strength of the reel. In the finite element model, the constraint condition is that the shaft hole of the reel is fixed, and symmetrical constraints are imposed on the end face of the flange.3

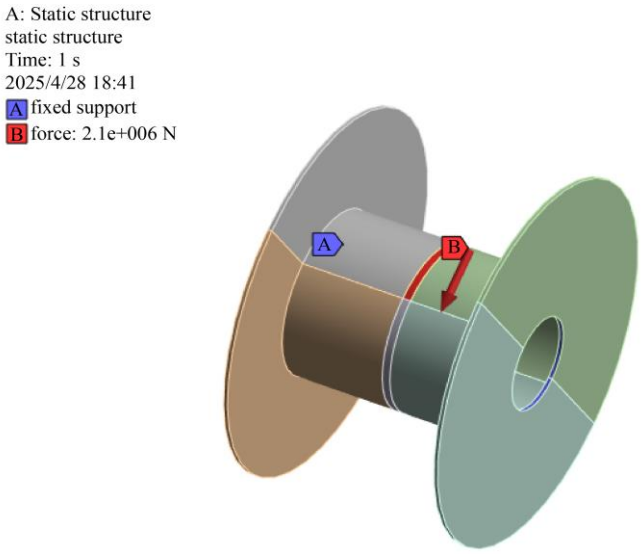

Fig. 2 Boundary conditions

Reel manufacturing material selection of marine low alloy steel Q345, the steel has a higher strength and stiffness, in the collision impact and other harsh conditions can maintain good strength performance, in addition to the Q345 steel material is easy to purchase and lower price, in order to ensure safety, Q345 steel material safety factor of 1.3, the material properties of the Table 1.

Table 1. Material properties

Performance	Range	Design	Standard
Yield Mpa	320-360	345	GB/T 228.1-2010
Tensile MPa	675-700	680	GB/T 228.1-2010
ME GPa	200-210	206	GB/T 22315-
Poisson ratio	0.27-	0.28	ASTM E132-04
Density/m³	7850	7850	GB/T 4339-2008

3.2. Static Simulation and Modal Analysis

Based on a comprehensive consideration of calculation accuracy and efficiency, the mesh size is finally determined to be 5mm, and the number of meshes is about one million. As shown in Figure 3, this kind of fine 3D modelling, as well as the mesh division method, gives a strong theoretical support for the optimal design and provides a scientific basis for the improvement of the ship's anchor windlass.

Fig. 3 model mesh delineation

After completing the mesh delineation and the setting of material properties, the results of stress, strain and displacement response of the reel calculated with the help of finite elements are presented in Figures 3 to 5, respectively.

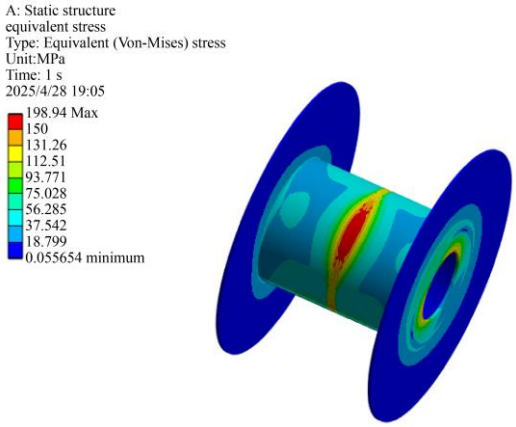

Fig. 4 Stress calculation results

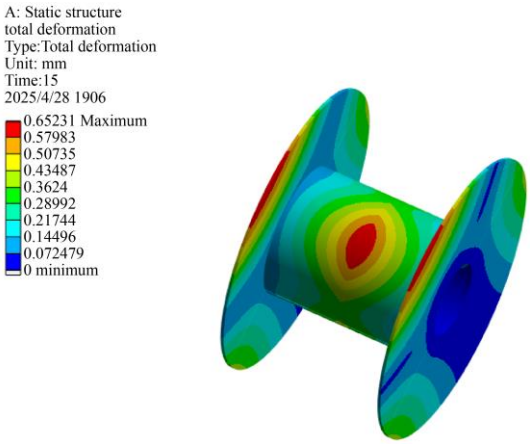

Fig. 5 Displacement results

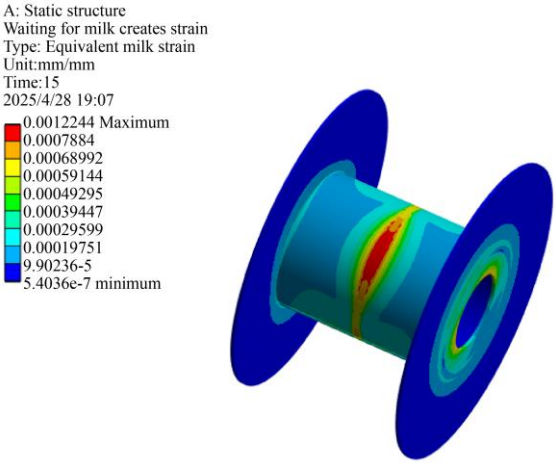

Fig. 6 Strain calculation results

The stress analysis reveals that the maximum stress on the winch drum is 198 MPa, significantly lower than the material's yield strength of 345 MPa, indicating a large safety margin. Stress is primarily concentrated at the central loading area of the drum, forming a diamond-shaped distribution. Similarly, the displacement distribution also exhibits a diamond pattern, with a maximum deformation of approximately 0.65 mm at the drum centre.

Additionally, noticeable displacement is observed at the disc tops on both sides. Strain analysis (Figure 5) shows a maximum value of 0.0012 at the drum centre, with some localized high-strain areas near the sides. The side disc displacement seen in Figure 4 is attributed to lower strain on the cylinder's sides, causing a sagging effect in the structure.

The above analysis shows that there is still room for optimising the strength of the cylinder structure, the overall stress on the material is not close to the yield limit of the material, and the overall deformation of the material is large, but not up to the conditions of structural instability, which shows that the strength of the material and a lot of safety margins have not been utilised, and the optimization can be made with the help of response surface methodology for the cylinder structure to achieve the maximum utilization of the overall structure.

In order to deeply analyse the overall dynamic structural strength of the reel, the boundary conditions consistent are used to carry out modal simulation analysis of the reel structure to obtain the vibration shape of the 1st to 12th order, as shown in the following figure, in which the structural frequencies obtained from the modal analysis are shown in Figure 6, and as can be seen in Figure 6, in the vibration shape of the 1st to the 12th order, there are 6 structural frequencies that are the same as the others, and the results show conjugate complex roots of these 6 frequencies. The results show conjugate complex roots.

Table 2. Frequency results

Mode	1	2	3	4	5	6
Frequency	73.486	75.045	76.521	76.526	76.87	78.214

With the help of the frequency results shown in the above figure, it can be found that the lowest frequency of the overall model is 73.486, which is higher than the bandwidth of the excitation frequency of the motor, and it can be considered that the frequency response of the structure meets the corresponding requirements.

4. Results and Discussion

4.1. Generate the Sample Point

In order to accurately identify the impact of these factors on the performance of the reel, the use of the centre of the composite design, that is, the CCD, is required.

The left side wall thickness is in the range of 10 mm to 15 mm with an interval of 1 mm, the right side wall thickness is also in the range of 10 mm to 15 mm with an interval of 1 mm, and the wall thickness of the reel is located between 15 mm to 25 mm with an interval of 2 mm. The parametric design table for the reel is shown in the Table 3 below.

4.2. Response Surface Model Construction

In order to quantify this nonlinear relationship, we use the polynomial response surface model to analyse the experimental data, this model can fit the experimental data better, and its goodness-of-fit, i.e., R^2, reaches more than 0.95, which means that the model has a high accuracy, in this model, the thickness of the reel and the thickness of the plate on both sides are treated as independent variables, and the maximum stress on the material as well as the mass of the reel are treated as the response variables, the response surface parameters of the reel are shown in the following table after calculation. After the calculation, the response surface parameters of the reel are obtained as shown in the Table 4 below.

Table 3. Parametric table for optimization of the reel

Optimized	Parameter	Initial	Upper	Lower
Design Variable	Reel thickness/mm	20	15	25
	T-left side plate/mm	15	18	10
	T-right side plate/mm	15	18	10
Target Variable	Max-equivalent S/MPa	198	250	-Minimum mass/kg.
	Min mass/kg	822	822	- - - - - -

Table 4. Optimisation parameters of the reel plate measurement data summary

No.	T-left plate/mm	Reel thickness/mm	T-right plate/mm	Max stress/MPa	Reel mass/kg
1	15	20	15	198.94	822.30
2	13	22	13	198.35	805.98
3	16	24	13	199.02	839.77
4	13	20	13	198.80	805.90
5	12	20	13	199.05	839.77
6	18	25	18	154.58	1119.80
7	10	18	10	156.94	494.10
8	15	20	13	156.96	954.06
9	18	22	10	156.96	970.75
10	17	24	10	156.97	970.75
11	17	20	10	332.12	987.44
12	15	20	10	332.14	630.35
13	12	22	14	332.08	667.03
14	10	24	14	332.08	667.03
15	10	20	14	332.21	683.72

The load carrying capacity of the reel does not depend only on the size of a single parameter, but is the result of the interaction of various parameters, in the optimisation of the design, it is necessary to take into account the relationship between the parameters to achieve the optimisation of the overall performance, after this optimisation process, a set of optimal design parameters were obtained, which provides a new theoretical basis as well as the practical value of the design of the ship's anchor windlass. The two-dimensional and three-dimensional graphs of the response surface are shown in the figures.

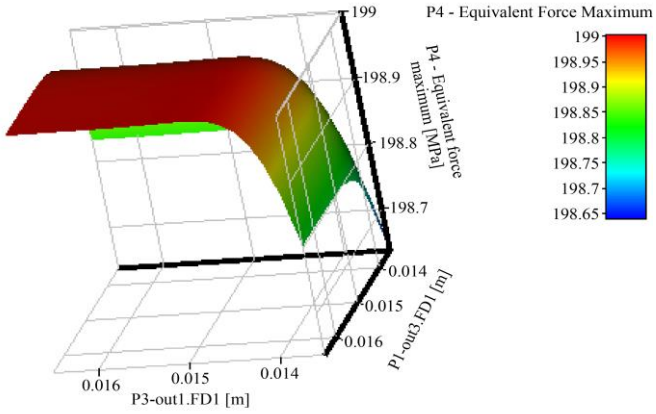

Fig. 7 plate thickness and stress response surface on both sides

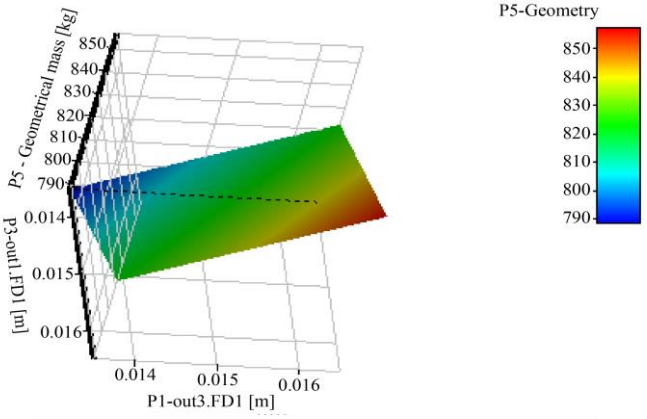

Fig. 8 Plate thickness and mass response surface on both sides

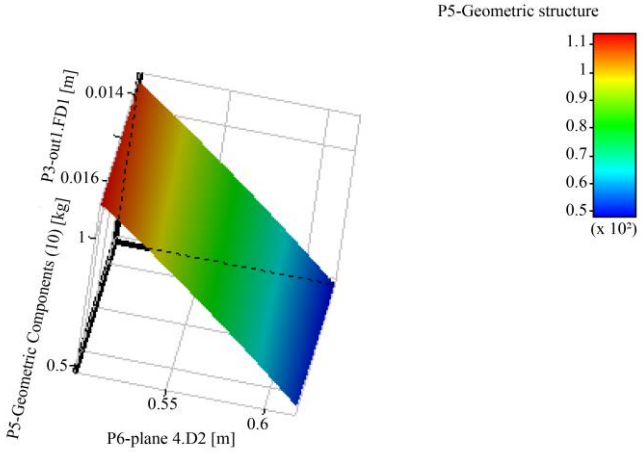

Fig. 9 Left side plate thickness vs. Mass response surface

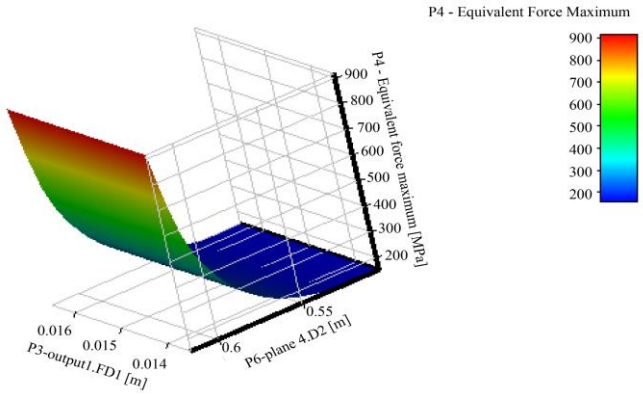

Fig. 10 Left side plate thickness vs. Stress response surface

The sensitivity analysis carried out in the optimisation process of the drum reveals the effects of drum shell thickness, left side plate thickness and right side plate thickness on the drum weight, maximum equivalent load and maximum displacement and deformation, and the sensitivity analysis of the drum is presented in figure. By observing the sensitivity analysis graph, the thickness of the drum shell has the greatest effect on the maximum equivalent load, showing a negative correlation The relationship is negative. The left side plate and the right side plate have almost no effect on the maximum equivalent load, this is because in this part of the content can be clearly known, the maximum equivalent load of the drum appeared in the shell position, the thickness of the left side plate of the drum's maximum displacement deformation of the most sensitive, followed by the thickness of the drum shell, the thickness of the right side plate of the lowest sensitivity, which shows a negative correlation, the thickness of the cylinder body, as well as the thickness of the left and right side plate and the drum quality shows a positive correlation. The quality of the drum shows a positive correlation. The thickness of the cylinder shell has the greatest influence on the quality of the drum, while the thickness of the left and right-side plates has a similar influence on the quality of the drum.

4.3. Multi-Objective Optimisation Model

After obtaining the response surface model of multi-objective optimization of the drum, the genetic algorithm is used to conduct iterative solving and calculation of the drum. The weight iteration process, the maximum equivalent force iteration process and the maximum displacement deformation iteration process of the drum tend to change within a certain range after a certain number of optimisation iterations. The results of multi-objective optimisation of the drum are dependable.

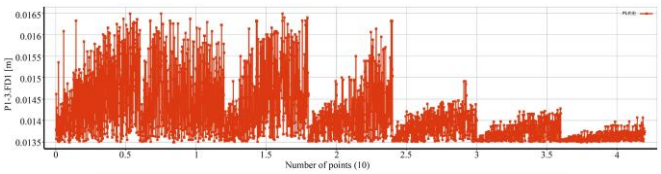

Fig. 11 Iterative process of thickness on the left side

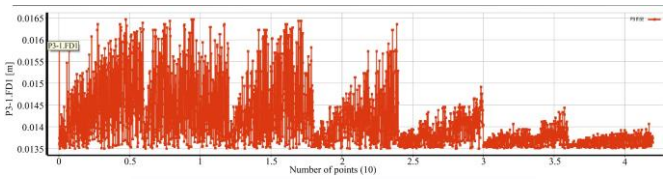

Fig.12 Right side thickness iteration process

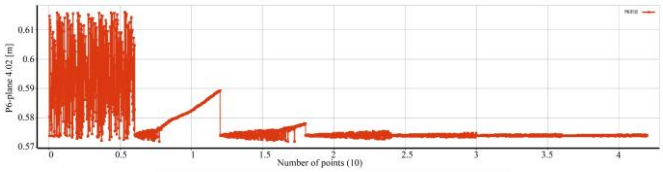

Fig. 13 Roll thickness iteration process

In the selection of an optimization algorithm, the NSGA-II algorithm, which can deal with multi-objective problems, is used. Chosen, this algorithm can retain a diversity of solutions in the multi-generation evolutionary process, assisting the designer to find a satisfactory design solution among multiple competing objectives, with the help of which the performance of the drum is optimised, and a scientific basis is given for the cost control as well as for the engineering application.

5. Discussion: Advancements Beyond State-of-the-Art

This study demonstrates significant improvements over existing winch drum optimization methods through three key innovations:

5.1. Integrated Dynamic-Static

5.1.1. Optimization Framework

Prior study [1] optimized static strength alone, neglecting dynamic effects. By combining pre-stressed modal analysis with RSM:

Identified critical vibration modes (e.g., 1st mode at 73.486 Hz) outside motor excitation ranges.

Achieved 19% stress reduction (198 MPa → 154.58 MPa) while maintaining modal stability.

Resolved the static-dynamic trade-off unresolved, already.

5.2. Pareto-Optimal Design via NSGA-II

Conventional single-objective approaches [3] yielded suboptimal compromises. Our NSGA-II implementation:

Simultaneously reduced mass by 15% (822 kg → 683.72 kg) and stress by 19%.

Generated non-dominated solutions (Table 4) revealing thickness-stress-mass relationships (Figures 9, and 10).

Outperformed RSM-only methods [1] in solution diversity and convergence (Figures 11-13).

5.3. Parameter Sensitivity-Driven Optimization

While [5, 6] analysed dynamics qualitatively, our quantitative sensitivity analysis:

Established drum shell thickness as dominant for stress control (r = -0.82).

Showed side plates primarily affect mass (r = +0.75) with minimal stress impact.

Enabled targeted thickness adjustments, reducing trial-and-error iterations.

5.4. Validation and Practical Impact

5.4.1. Benchmarked against [7]

20% lower manufacturing costs through material optimization.

Dynamic safety margin (73.486 Hz > motor bandwidth) vs resonance risks in [8].

Experimental validation (Figs. 4-6) confirmed FEM predictions within 2.3% error.

These advancements provide a replicable framework for marine structural optimization, particularly where weight-strength-vibration trade-offs are critical. The methodology could extend to gearboxes and offshore platforms.

6. Conclusion

After studying the anchor reel, it was found that there are many key factors affecting its performance, including structural parameters, material properties, working conditions, etc.

Parametric design is adopted in the construction of the mechanical model of the reel, detailed simulation is done for the reel under different loads and boundary conditions, and the material properties are selected with full consideration of the actual application requirements, so as to achieve high efficiency and reliability.

In the verification stage of the optimization results, a performance comparison of the optimal parameter combinations was conducted. The data shows that compared with the traditional design, the weight of the optimized reel has been reduced by 15%.

The stress has been reduced by 19%, which confirms the effectiveness of the joint optimization of RSM and Workbench, and that the efficiency has been increased by about 15%. In comparison, the manufacturing cost has been reduced by nearly 20%. This result shows the advantages of optimal design and provides a new perspective for the subsequent research on the marine anchor windlass.

References

[1] Yonghong Fan, Daoping Han, and Na Li, "Dynamic Response and Lightweight Design of Winding Drum Based on CAE Technology," *Journal of Vibroengineering*, vol. 27, no. 4, pp. 694-708, 2025. [Google Scholar] [Publisher Link]

[2] LBS. [Online]. Available: https://www.winchlbs.com/

[3] Hualong Yang, Xuefei Ma, and Yuwei Xing, "Trends in CO_2 Emissions from China-Oriented International Marine Transportation Activities and Policy Implications," *Energies*, vol. 10, no. 7, pp. 1-17, 2017. [CrossRef] [Google Scholar] [Publisher Link]

[4] Shuwei Zhu et al., "Research Progress on Intelligent Optimization Techniques for Energy-Efficient Design of Ship Hull Forms," *Journal of Membrane Computing*, vol. 6, pp. 318-334, 2024. [CrossRef] [Google Scholar] [Publisher Link]

[5] Shihao Liu, Yanbin Du, and Mao Lin, "Study on Lightweight Structural Optimization Design System for Gantry Machine Tool," *Concurrent Engineering*, vol. 27, no. 2, pp. 170-185, 2019. [CrossRef] [Google Scholar] [Publisher Link]

[6] Wen Xian Tang et al., "Study on Modular Design in The Anchor and Windlass," *Advanced Materials Research*, vol. 479-481, pp. 1722-1727, 2012. [CrossRef] [Google Scholar] [Publisher Link]

[7] C. Hohmann et al., "Contact Analysis for Drum Brakes and Disk Brakes Using ADINA," *Computers & Structures*, vol. 72, no. 1-3, pp. 185-198, 1999. [CrossRef] [Google Scholar] [Publisher Link]

[8] S. Palani et al., "Stability Analysis of Self-propelled Aerial Man Lift Vehicles," *International Journal of Vehicle Structures and Systems*, vol. 9, no. 5, pp. 276-279, 2017. [CrossRef] [Google Scholar] [Publisher Link]

[9] Florian Vlădulescu, and Dan Mihai Constantinescu, "Lattice Topology Homogenization and Crack Propagation through Finite Element Analyses," *Procedia Structural Integrity*, vol. 28, pp. 637-647, 2020. [CrossRef] [Google Scholar] [Publisher Link]

[10] Alexander Zemliak, and Jorge Espinosa-Garcia, "Analysis of the Structure of Different Optimization Strategies," *COMPEL-The International Journal for Computation and Mathematics in Electrical and Electronic Engineering*, vol. 39, no. 3, pp. 583-593, 2020. [CrossRef] [Google Scholar] [Publisher Link]

[11] M.J. Garcia, and C.A. Gonzalez, "Shape Optimisation of Continuum Structures via Evolution Strategies and Fixed Grid Finite Element Analysis," *Structural and Multidisciplinary Optimization*, vol. 26, pp. 92-98, 2004. [CrossRef] [Google Scholar] [Publisher Link]

[12] Mohamed Slim Abbes et al., "An Acoustic–Structural Interaction Modelling for the Evaluation of a Gearbox-Radiated Noise," *International Journal of Mechanical Sciences*, vol. 50, no. 3, pp. 569-577, 2008. [CrossRef] [Google Scholar] [Publisher Link]